J Porous Mater
DOI 10.1007/s10934-008-9227-6

New hydroxyapatite–hydrotalcite composites I. synthesis

J. A. Rivera · G. Fetter · L. Baños · J. Guzmán · P. Bosch

© Springer Science+Business Media, LLC 2008

Abstract The synthesis and characterization of original materials, composed by hydrotalcite and hydroxyapatite, is discussed. All the syntheses were carried out in presence of microwave irradiation during the crystallization step. The interactions between the two compounds depend on the synthesis procedure. If hydroxyapatite is incorporated to hydrotalcite, the first compound is encapsulated by hydrotalcite. Instead, if hydroxyapatite is first prepared, the resulting solid is essentially a hydrotalcite with interlayered hydroxyapatite. When the composite material is synthesized by a simultaneous coprecipitation, the small clusters of hydroxyapatite and hydrotalcite are homogeneously dispersed. Consequently, the specific surface area and the particle size vary.

Keywords Hydrotalcite · Hydroxyapatite · Composite · Microwave irradiation · Biomaterial · Catalyst · Bone

1 Introduction

Homogeneous catalysis is a polluting process where the reactants are hardly separated from products and catalysts. Thus, heterogeneous processes are always preferred. In aldol condensation reactions, the carbanion is generated through the abstraction of a hydrogen alpha from acetone to form a carbonyl group. This reaction may be catalyzed by bases as sodium hydroxide, sodium ethoxide or ammines in homogeneous phase [1]. A solid base is hydrotalcite, whose chemical formula is [2, 3]:

$$\left[M^{2+}_{1-x}M^{3+}_{x}(OH)_2\right](A^{m-})_{x/m}\cdot nH_2O$$

where M^{2+} may be replaced by three-valent atoms, M^{3+}, which produce positively charged layers. This charge is neutralized by A, a compensating anion with charge m^- as CO_3^{2-} or NO_3^-. Metal ratio M^{2+}/M^{3+}, concentration of reactants and the synthesis procedure (sol–gel, ultrasound or microwave irradiation, among others) determine the properties of hydrotalcite-like compounds [4–10]. Hydrotalcites are versatile lamellar compounds.

Often, a bi-functionality is required where the acid and base characters should be present in the same catalyst. In this sense, hydrotalcite could be combined with a solid presenting an acidic feature. Hydroxyapatite, $Ca_{10}(PO_4)_6(OH)_2$, is a cationic exchanger which has been used to anchor ruthenium complexes [11] or to support Ni–Mo sulphides [12]. Such composites could be used in medicine, indeed, hydrotalcite and hydroxyapatite are well known biomaterials. They are related compounds as they are both solid hydroxides which present ion exchange properties.

Poorly crystalline hydroxyapatite is the main mineral component of bone and other physiologically calcified tissues. In orthopedics, it seems that the best material for replacing a bone tissue has to be identical to that tissue, concept known as biomimicry [13]. Hydroxyapatite has to be incorporated as small clusters in order to promote the self organizing processes of biomineralization [14]. Furthermore, small hydroxyapatite particles supported on a biocompatible material should provide a solid adequate to

J. A. Rivera · G. Fetter (✉)
Facultad de Ciencias Químicas, Universidad Autónoma de Puebla, Blvd. 18 Sur y Av. San Claudio, C.P. 72570 Puebla, PUE, Mexico
e-mail: geolarfetter@yahoo.com.mx

L. Baños · J. Guzmán · P. Bosch
Instituto de Investigaciones en Materiales, Universidad Nacional Autónoma de México, 04510 Mexico, DF, Mexico

distribute and dose hydroxyapatite in the organism or straightforward into the damaged zone [15].

If, the other way round, the hydrotalcite particles are on the hydroxyapatite surface, the hydrotalcite would have the role of a drug dispenser. Indeed, it is used as an antiacid medicine and it has been already shown that the nitrate form of anionic clay is a potential candidate for the development of slow-release nitrate fertilizer [16].

Hence, the proposed hydroxyapatite–hydrotalcite materials could be used in catalysis as well as in biomedicine, among others. In the first field, as already discussed, the important feature would be the acid–base character whereas, in the second, the morphology and the interaction between the two hydroxides is the relevant property. In this work, we correlate the synthesis procedure with the structural and textural features of the hydroxyapatite–hydrotalcite composites.

2 Experimental

2.1 Preparation

2.1.1 Hydroxyapatite synthesis

The hydroxyapatite sample (sample HA) was prepared from a 0.8 M (Baker) H_3PO_4 solution dropped in a 2 M (Baker) $Ca(OH)_2$ solution adjusting the flow in such a way that the pH was maintained constant and equal to 11.5. The amount of reactants was such that the molar ratio Ca/P was equal to 1.67. The mixture was introduced in a microwave autoclave (MIC-I Sistemas y Equipos de Vidrio S.A. de C.V.) for 10 min. The used frequency was 2.45 GHz, power of 200 W, temperature of 80 °C and pressure of 1 atm. Note that this autoclave model is provided with an automatic valve that maintains constant the selected pressure. The sample was washed with distilled water until the waste water reached a pH 10. Solids were recovered by decantation and dried in an oven at 70 °C.

2.1.2 Hydrotalcite synthesis

Mg/Al hydrotalcite sample (sample HT) was synthesized from Mg- and Al-nitrate water solutions, 2.5 M and 2 M NaOH. The flow of each solution was adjusted so that the pH was constant at 11.5. The amounts correspond to a molar ratio Mg/Al of 2. The resulting gel was treated in the microwave autoclave for 10 min operating at 2.45 GHz. The power was 200 W and the temperature was fixed at 80 °C. The solid was recovered by decantation and washed with distilled water up to a waste water pH value of 10 and dried in an oven at 70 °C.

2.1.3 Hydrotalcite incorporation to hydroxyapatite

Over the hydroxyapatite previously prepared, before decantation, a solution of magnesium and aluminum nitrates, 2.5 M for each metal, was dropped simultaneously with a 2.0 M NaOH solution to maintain the pH value equal to 11.5. The amounts were such that the Mg/Al ratio was 2. The resulting mixture was submitted to microwave irradiation for 10 min as previously. The sample (sample HT–HA) was washed up to pH 10 and dried at 70 °C, as previously.

2.1.4 Hydroxyapatite incorporation to hydrotalcite

The previous solution used to prepare hydroxyapatite was employed, before decantation of the already prepared hydrotalcite, following the same procedure as in the incorporation of hydrotalcite to hydroxyapatite (sample HA–HT).

2.1.5 Simultaneous synthesis

Both hydrotalcite and hydroxyapatite precursor solutions were dropwise mixed at constant pH of 11.5. After the coprecipitation the sample was treated in the microwave autoclave for 10 min at 80 °C. The recovered solid was washed in distilled water and dried at 70 °C (sample AT).

In all composite materials the molar ratio hydroxyapatite/hydrotalcite was 1.

2.2 Characterization

2.2.1 X-ray diffraction

A Bruker-axs D8-advance diffractometer coupled to a copper anode X-ray tube was used to identify the compounds present in the powdered samples. A diffracted beam monochromator selected the Kα radiation.

2.2.2 FTIR spectroscopy

FTIR spectra in the region 4,000–400 cm^{-1} were obtained with a Magna-IR Spectrometer 550 Nicolet. The pellets were prepared with KBr.

2.2.3 Nitrogen adsorption

The BET surface areas were determined from the nitrogen adsorption–desorption curves by the conventional multipoint technique with a Micromeritics ASAP 2020. The samples were pretreated at 200 °C for 10 h at high vacuum. The pore size distribution curves were obtained by the BJH method applied to the desorption branch.

2.2.4 Scanning electron microscopy

A scanning electron microscope LEICA, Stereoscan 440 was used. The samples were previously covered with gold to avoid charge problems.

3 Results

3.1 Hydroxyapatite (sample HA)

The X-ray diffraction peaks of the prepared hydroxyapatite are sharp and intense, figure not shown, revealing that the material is highly crystalline. All the diffraction peaks can be attributed to hydroxyapatite (JCPDS card 09-0432) whose symmetry is hexagonal. No preferred orientations are observed as the intensities reproduce those reported in the JCPDS card.

In the infrared spectrum, Fig. 1, the phosphate bands were found at 1104, 1042, 955, 604, 578 and 469 cm^{-1} [17, 18]. The intense band at 3,454 cm^{-1} corresponds to the stretching vibration of OH groups present in the hydroxyapatite structure. The flexion vibration of those groups appears at 1,644 cm^{-1}. The bands at 1,427 and 874 cm^{-1} may be attributed to small amounts of CO_3^{2-} which are formed by atmospheric CO_2 molecules reacting with the alkaline solutions.

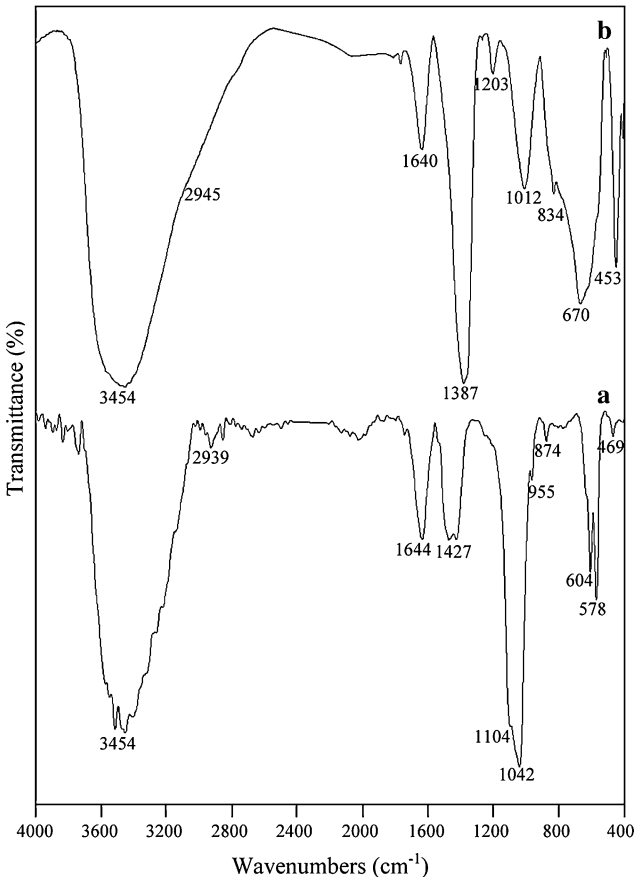

Fig. 1 Infrared spectra of the hydroxyapatite HA (**a**) and the hydrotalcite HT (**b**) samples

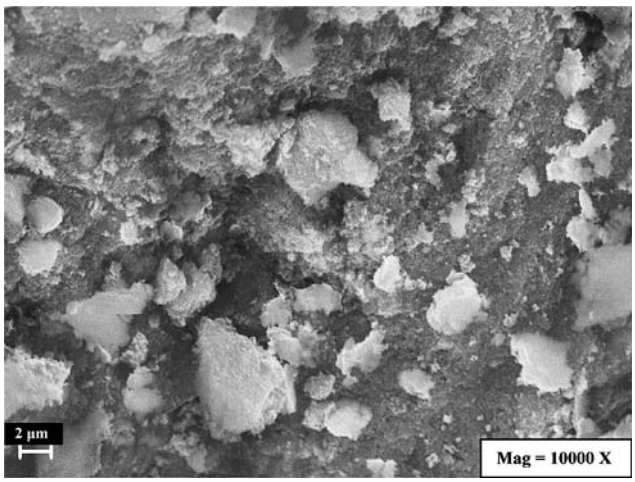

Fig. 2 Scanning electron micrograph of the sample HA

The morphology of the hydroxyapatite prepared in presence of microwave irradiation, Fig. 2, is not homogeneous. The grains are irregular and their mean size could be ca. 5 µm. The grain surface reveals the presence of much smaller particles ca. 0.2 µm.

The nitrogen adsorption–desorption isotherm, Fig. 3, presents a hysteresis loop starting at $P/P_0 = 0.65$, type H1 (IUPAC classification), thus, the pores are ink-bottle shaped and cylindrical channels open in both extremes. This curve can be recognized as a Type IV isotherm (also from IUPAC classification), showing that the sample is mesoporous. The pore size distribution, Fig. 4, is very broad, from 20 to 340 Å. The maximum of the distribution is found for a diameter of 240 Å (mesopores). The obtained specific surface area is 112 m^2/g; this value is much higher than the one reported by Smahi et al. [19] obtained in a conventionally prepared material. Irradiation is expected to propitiate seed formation and hence to favor small particle sizes and, thus, high specific surface areas are expected [7, 20–22].

3.2 Hydrotalcite (sample HT)

The X-ray diffractogram, figure not shown, reveals the presence of a well crystallized hydrotalcite (JCPDS card 35-0965) whose symmetry is hexagonal. All the peaks of the prepared hydrotalcite overlap with those of the hydroxyapatite. However, the 003 peak of hydrotalcite is much more intense than the 100 hydroxyapatite peak. Thus, the presence of hydrotalcite can be inferred from the observation of this region of the X-ray diffraction pattern.

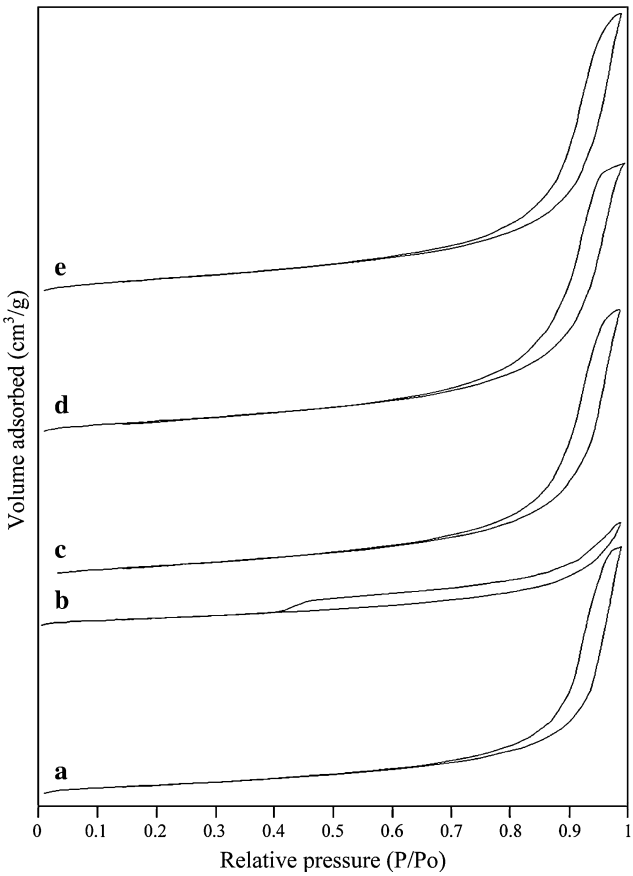

Fig. 3 Nitrogen adsorption–desorption isotherms of the samples HA (**a**), HT (**b**), HT–HA (**c**), HA–HT (**d**) and AT (**e**)

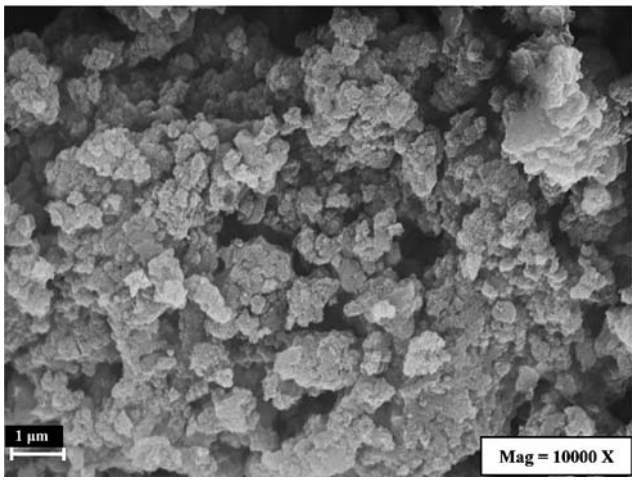

Fig. 5 Scanning electron micrograph of the sample HT

The infrared spectrum, Fig. 2, presents the bands of the well known groups present in hydrotalcite [20, 23]. The band at 3,454 cm^{-1} corresponds to an elongation vibration of structural hydroxyl groups. The band at 1,640 cm^{-1} is due to OH groups from water molecules, and the interlayered nitrates appear at 1,687 cm^{-1}. A broad band from 500 to 900 cm^{-1} can be attributed to metal-oxygen vibrations, the vibration of Al–O band is found at 1,012 cm^{-1} and the vibration of Mg–O at 670 cm^{-1} [24].

Figure 5 shows the typical hydrotalcite morphology whose size is close to 0.3 µm [21, 22]. The grains are constituted by hexagonally shaped layers stacked in small groups. Then, hydrotalcite can be easily differentiated from hydroxyapatite through the corresponding morphologies.

The shape of the nitrogen adsorption–desorption curve corresponds to a Type IV isotherm, Fig. 3. Again, the solid is mesoporous. Such qualitative observation agrees with the pore size distribution presented in Fig. 4. The

Fig. 4 Pore size distributions of the samples

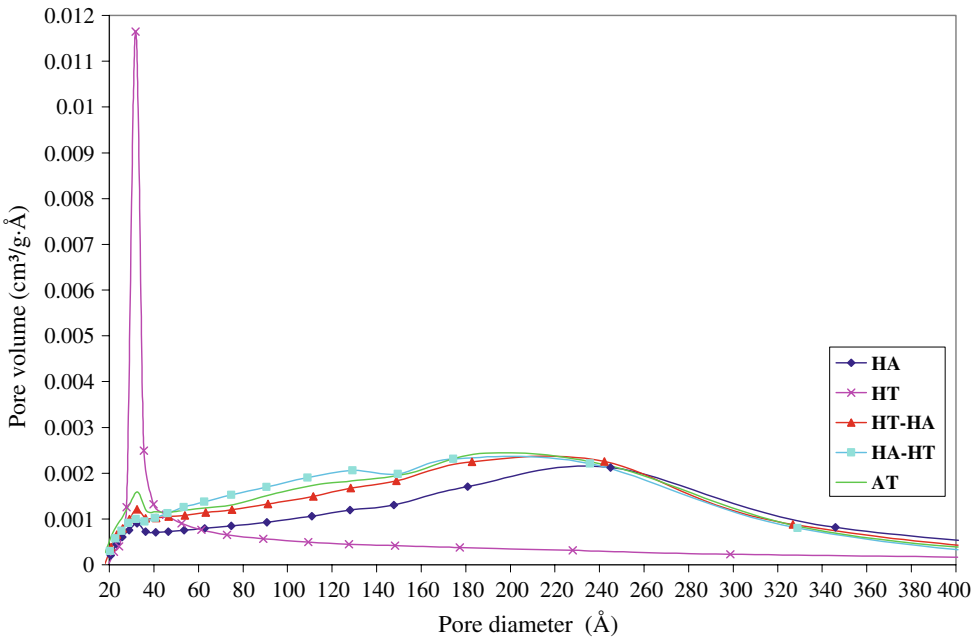

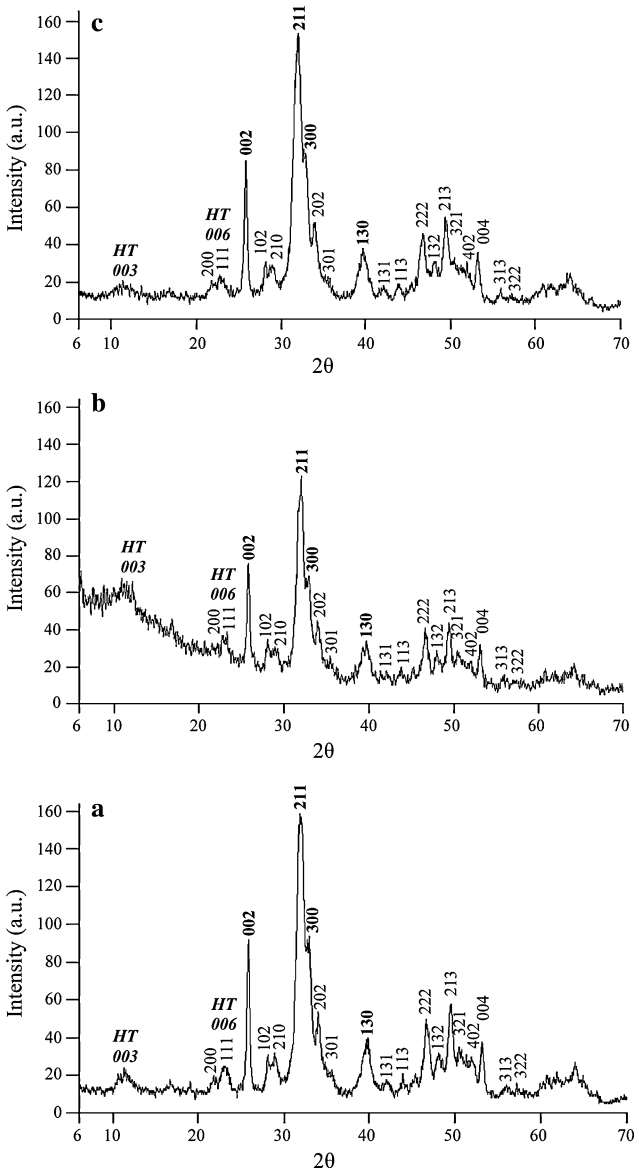

Fig. 6 X-ray diffraction patterns of the composites HT–HA (**a**), HA–HT (**b**) and AT (**c**)

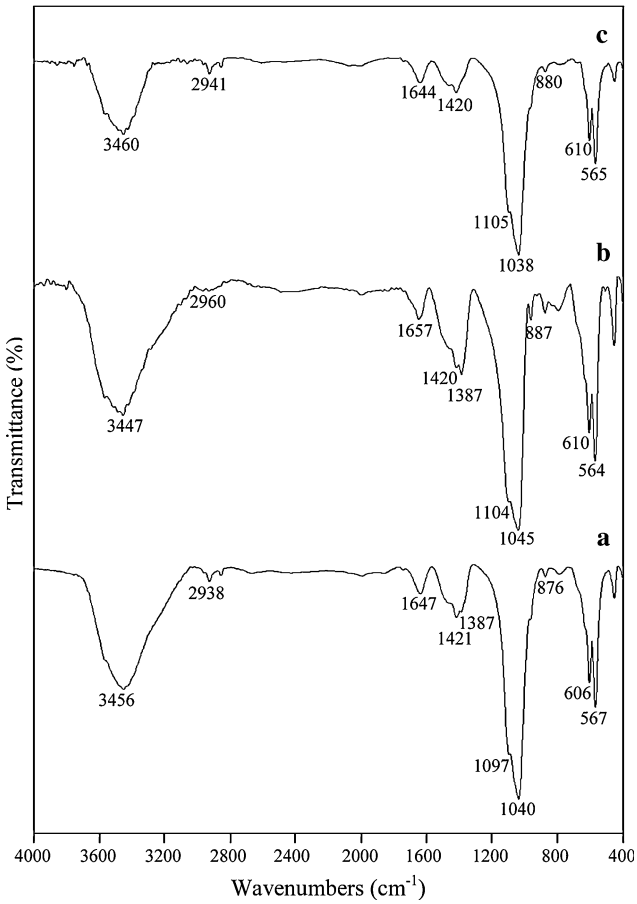

Fig. 7 Infrared spectra of the composites HT–HA (a), HA–HT (b) and AT (c)

distribution is monomodal with a maximum at 30 Å. This porosity corresponds to interstitial spaces between the hydrotalcite crystallites. In this sample the isotherm turns out to be type H4, attributed to a porous system due to parallel layers and lamellae. The specific surface area is 89 m^2/g.

3.3 Hydrotalcite/hydroxyapatite (sample HT–HA)

The X-ray diffraction pattern of the HT–HA sample, Fig. 6, can be interpreted in terms of hydroxyapatite and hydrotalcite. The X-ray diffraction peaks of the hydroxyapatite are sharp and well defined revealing a crystalline hydroxyapatite. The hydroxyapatite is not altered by the preparation procedure. In the zone 10 to 12° (2θ), the peak 100 of the hydroxyapatite appears more intense and broad. This difference is attributed to the superimposed 003 hydrotalcite interplanar distances.

The infrared spectra, Fig. 7, present the typical bands of hydroxyapatite already discussed. The intense band from 1,300 to 1,560 cm^{-1} is constituted by three peaks instead of the two present in pure HA. The peak at 1,387 cm^{-1} is attributed to the disordered nature of interlamellar ions in the hydrotalcite [3]. This observation supports the presence of surface hydrotalcite particles, Fig. 8.

The scanning electron micrograph, Fig. 8, shows two grain morphologies, on the one hand, large particles similar to those reported for HA sample and by other authors [13], on the other, small agglomerates growing in the intergranular spaces which correspond to hydrotalcite (grain size lower than 1 μm).

Figure 3 compares the nitrogen adsorption–desorption curves, the HT–HA presents a clear hysteresis loop similar to that of the HA sample. Therefore, the adsorption behavior is determined by the hydroxyapatite porosity. Such conclusion is in agreement with the corresponding pore size distribution, Fig. 4. Indeed, a broad distribution

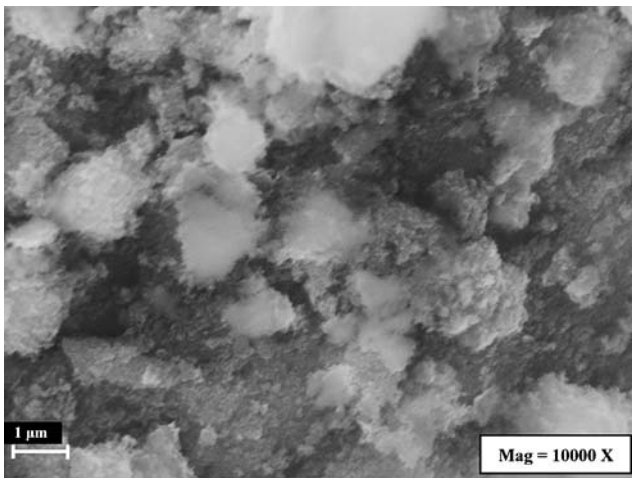

Fig. 8 Scanning electron micrograph of the sample HT–HA

was obtained centered at 220 Å and a small peak at 30 Å. The specific surface area of this composite material turned out to be 143 m^2/g. This value is higher than the area obtained for the hydroxyapatite (112 m^2/g) due to the hydrotalcite contribution. As the molar ratio hydroxyapatite/hydrotalcite was one, the corresponding surface area of a weighted mixture could be estimated and the obtained value was 98 m^2/g. Hence, the adsorption properties of the obtained sample cannot be interpreted as a simple addition of hydrotalcite and hydroxyapatite contributions.

3.4 Hydroxyapatite/hydrotalcite (sample HA–HT)

Both crystalline phases are present in this composite as shown by the X-ray diffraction pattern, Fig. 6. It has to be emphasized that the hydrotalcite peak is much more intense than in the previous sample, although the nominal amounts of hydroxyapatite and hydrotalcite are the same. Then, in this material, hydrotalcite particles are more crystalline than in the inverse preparation (sample HT–HA). Indeed, hydroxyapatite is precipitated on the already crystallized hydrotalcite.

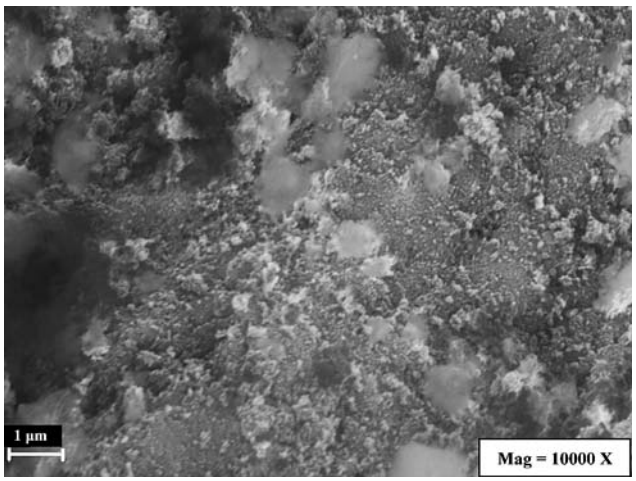

Fig. 9 Scanning electron micrograph of the sample HA–HT

The infrared spectrum of HA–HT sample, Fig. 7, does not significantly differ from HT–HA and AT samples, only the nitrate content seems to be higher as the band at 1,387 cm^{-1} is more intense [25, 26]. The same band may be used to detect the presence of well ordered hydrotalcite as nitrates and some carbonates are the compensating ions in that compound [16]. Then, only in this sample (HA–HT) the hydrotalcite forms a well ordered layered compound.

The SEM image, Fig. 9, presents large grains attributed to hydroxyapatite covered inhomogeneously by small particles (less than 0.1 μm). These small particles (hydrotalcite) are distributed in the intergranular spaces left by the hydroxyapatite grains. They often associate as concentric ensembles.

The profile of the hysteresis loop in the adsorption–desorption curve of this sample, Fig. 3, is similar to that of the previous preparation (HT–HA). As the type is IV and H2, the pores are mainly due to interstices between lamellae, then, the material is dense. The pore size distribution, Fig. 4, reveals not only the presence of large mesopores (200 Å) but also pores of 30 Å. The specific surface area obtained in this sample is 144 m^2/g.

3.5 Simultaneous synthesis (sample AT)

If the precursor solutions are mixed, the main compound identified by X-ray diffraction, Fig. 6, is hydroxyapatite. The peaks corresponding to hydrotalcite are broad and small. Thus, a large number of hydrotalcite-like crystallites must be undetected by X-ray diffraction. They are, therefore, smaller than 30 Å, detection limit of the technique.

In the infrared spectrum of Fig. 7, a well defined band at 2,941 cm^{-1}, found also in the other composites, but with lower intensity, reveals the presence of a bond anion-water through a hydrogen bridge between the hydrotalcite lamellae. It has to be emphasized that the band at 1,387 cm^{-1}, attributed to hydrotalcite interlayered nitrate, is significantly diminished. Thus, hydrotalcite is partially delaminated.

The SEM image, Fig. 10, presents small, less than 0.05 μm, and homogeneous particles assembled very loosely forming a cloud-like network. Note that the smooth and large surfaces, due to pure hydroxyapatite, are not observed, therefore hydroxyapatite particles are totally covered by hydrotalcite clusters.

The nitrogen isotherm profile of this sample, Fig. 3, reproduces the HT–HA curve. Then, the same conclusions can be reached: ink-bottle shaped pores and interstitial mesopores between lamellae. Again, the pore size

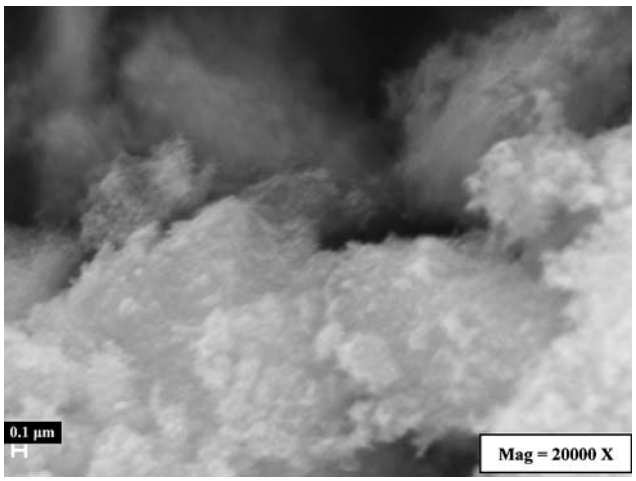

Fig. 10 Scanning electron micrograph of the sample AT

distribution reproduces the pore size distribution of the HT–HA sample. As expected from the X-ray diffraction pattern (broad peaks indicating small particles) and the SEM image (very small and loosely bonded aggregates), the specific surface area (156 m^2/g) is the highest if compared to those of the previous samples. It is in agreement with the high dispersion and low size of the hydrotalcite crystallites.

4 Discussion

From XRD, nitrogen adsorption–desorption and SEM results the HA and the HT samples may be clearly differentiated, as hydroxyapatite presents large crystals and a broad pore size distribution. Instead, hydrotalcite has broad diffraction peaks, a narrow and monomodal pore size distribution (30 Å) and a morphology constituted by small grains often hexagonal and layered. In previous works, it has been shown that the microwave treatment produces small hydrotalcite crystals [27, 28]. In HT sample, the specific surface area is 112 m^2/g, but, in HT sample, it turns out to be smaller, 89 m^2/g.

In the composite materials, the preparation sequence determines the morphology and the distribution of hydroxyapatite and hydrotalcite. If the hydroxyapatite is first prepared, small hydrotalcite crystals are obtained, instead if the hydrotalcite is the initial compound the crystal size of both hydroxyapatite and hydrotalcite is larger. Only when the synthesis is simultaneous, a close and homogeneous interaction between hydroxyapatite and hydrotalcite is obtained. Although in this material hydroxyapatite crystallizes first as its solubility product is much smaller (Kps (hydrotalcite) = 10^{-11} and Kps (hydroxyapatite) = 10^{-117}) [29], the sample is constituted by a hydroxyapatite core and a shell of hydrotalcite small crystals fairly homogeneous. Indeed, in these conditions the negatively charged hydroxyapatite small nuclei first formed attract the positively charged hydrotalcite layers, hydrotalcite crystallizes but remains partially delaminated as shown by infrared spectra. It seems that the interaction hydrotalcite–hydroxyapatite is stronger than that of the hydrotalcite–hydrotalcite layers; therefore, hydrotalcite distributes around and between hydroxyapatite nuclei.

Even if the crystalline symmetries are hexagonal, an epitaxial growth or a strong interaction between planes is difficult as the cell parameters are very different. In hydrotalcite, the **a** cell parameter is three times smaller

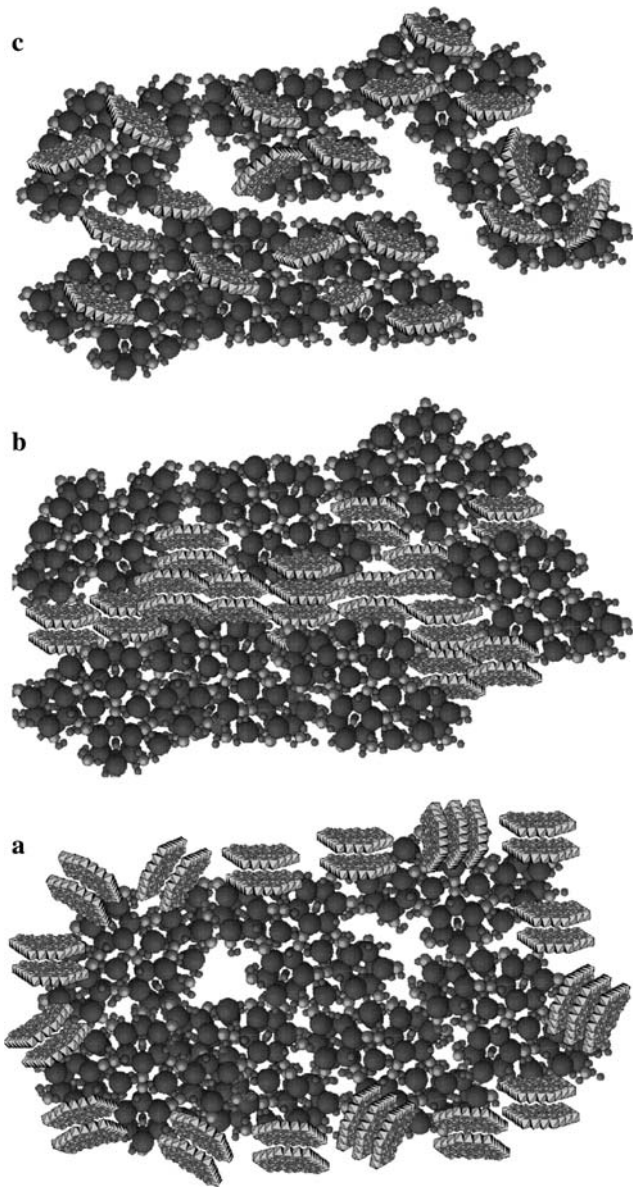

Schema 1 Structural representation of the composites: (**a**) hydrotalcite incorporated to hydroxyapatite; (**b**) hydroxyapatite incorporated to hydrotalcite and (**c**) simultaneous precipitation of hydrotalcite and hydroxyapatite

than in hydroxyapatite; in the **c** direction it is almost four times larger (HT: a = 3.05 Å, c = 23.40 Å; HA: a = 9.46 Å, c = 6.87 Å). Such point is most relevant as interplay between stereochemical, structural, or electrostatic properties of a specific crystal face governs the interaction of macromolecules and crystals in biomineralization [15]. In catalysis, crystallographic planes, as well as edge atoms, are known to determine the high selectivity of small particles through an electronic effect. Furthermore, not only the particle size is relevant but also the density of structural defects which, again, present electronic deficiencies [30].

5 Conclusion

Modifying synthesis methods, various composite materials were obtained whose structure, texture and morphology are unique and determined by the interaction between hydroxyapatite and hydrotalcite. Such an interaction determines the porosity or the surface area, as well as the particle size. The various structures are summarized in Schema 1. As shown, the interaction between hydrotalcite and hydroxyapatite can be tailored with the preparation sequence. These new materials should be useful in bifunctional catalysis, as basicity and acidity should be most different. In biomedicine, they should be adequate to combine hydroxyapatite deliverance with a drug dispenser hydrotalcite.

Acknowledgements The authors gratefully acknowledge the financial support of CONACYT.

References

1. F. Prinetto, D. Tichit, R. Teissier, B. Coq, Catal. Today **55**, 103 (2000). doi:10.1016/S0920-5861(99)00230-8
2. V. Rives, M.A. Ulibarri, Coord. Chem. Rev. **181**, 61 (1999). doi:10.1016/S0010-8545(98)00216-1
3. F. Cavani, E. Trifiro, A. Vaccari, Catal Today **11**, 173 (1991). doi:10.1016/0920-5861(91)80068-K
4. Y.F. Wang, H.Z. Gao, J. Colloid Interface Sci. **301**, 19 (2006)
5. J.A. Rivera, G. Fetter, P. Bosch, Microporous Mesoporous Mater. **89**, 306 (2006). doi:10.1016/j.micromeso.2005.10.041
6. J.A. Rivera, G. Fetter, Y. Jiménez, M.M. Xochipa, P. Bosch, Appl. Catal. A **316**, 207 (2007). doi:10.1016/j.apcata.2006.09.031
7. S.P. Paredes, G. Fetter, P. Bosch, S. Bulbulian, J. Mater. Sci. **41**, 3377 (2006). doi:10.1007/s10853-005-5347-4
8. L. Du, B. Qu, Polym. Compos. **28**, 131 (2007). doi:10.1002/pc.20279
9. M.J. Climent, A. Corma, S. Iborra, K. Epping, A. Velti, J. Catal. **225**, 316 (2004). doi:10.1016/j.jcat.2004.04.027
10. S. Komarneni, Q.H. Li, R. Roy, J. Mater. Res. **11**, 1866 (1996). doi:10.1557/JMR.1996.0236
11. K. Mori, T. Hara, T. Mizugaki, K. Ebitani, K. Kaneda, J. Am. Chem. Soc. **125**, 11460 (2003). doi:10.1021/ja0302533
12. N. Elazarifi, M.A. Chaoui, A.E. Ouassouli, A. Ezzamarty, A. Travert, J. Leglise et al., Catal. Today **98**, 161 (2004). doi:10.1016/j.cattod.2004.07.030
13. W. Bonfield, M. Wang, K.E. Tanner, Acta Mater. **46**, 2509 (1998). doi:10.1016/S1359-6454(98)80035-9
14. P. Simon, U. Schwarz, R. Kniep, J. Mater. Chem. **15**, 4992 (2005). doi:10.1039/b504977f
15. K. Flade, C. Lau, M. Mertig, W. Pompe, Chem. Mater. **13**, 3596 (2001). doi:10.1021/cm011063z
16. J. Olanrewaju, B.L. Newalkar, C. Mancino, S. Komarneni, Mater. Lett. **45**, 307 (2000). doi:10.1016/S0167-577X(00)00123-3
17. N. Pleshko, A. Boskey, R. Mendelsohn, Biophys. J. **60**, 786 (1991)
18. J. Liu, X. Ye, H. Wang, M. Zhu, B. Wang, H. Yan, Ceram. Int. **29**, 629 (2003). doi:10.1016/S0272-8842(02)00210-9
19. A. Smahi, A. Solhy, H. el Badaoui, A. Amoukal, A. Tikad, M. Maizi et al. Appl. Catal. **250**, 151 (2003). doi:10.1016/S0926-860X(03)00254-0
20. H. Katsuki, S. Furuta, J. Am. Ceram. Soc. **82**, 2257 (1999)
21. P. Benito, F.M. Labajos, V. Rives, J. Solid State Chem. **179**, 3784 (2006). doi:10.1016/j.jssc.2006.08.010
22. O. Bergadà, I. Vicente, P. Salagre, Y. Cesteros, F. Medina, J.E. Sueiras, Microporous Mesoporous Mater. **101**, 363 (2007). doi:10.1016/j.micromeso.2006.11.033
23. S.L. Wang, C.T. Johnston, Am. Mineral **85**, 739 (2000)
24. T. López, P. Bosch, M. Asomoza, R. Gómez, E. Ramos, Mater. Lett. **31**, 311 (1997). doi:10.1016/S0167-577X(96)00296-0
25. S. Milev, G.S. Kannangara, M.A. Wilson, Langmuir **20**, 1888 (2004). doi:10.1021/la0355601
26. M. Uota, H. Arakawa, N. Kitamura, T. Yoshimura, J. Tanaka, T. Kijima, Langmuir **21**, 4724 (2005). doi:10.1021/la050029m
27. G. Fetter, A. Botello, V.H. Lara, P. Bosch, J. Porous Mater. **8**, 227 (2001). doi:10.1023/A:1012292807651
28. B. Zapata, P. Bosch, G. Fetter, M.A. Valenzuela, J. Navarrete, V.H. Lara, Int. J. Inorg. Mater. **3**, 23 (2001). doi:10.1016/S1466-6049(00)00097-0
29. F.C.M. Driessens, R.M.H. Verbeeck *Biominerals*, (CRC Press, 2000), p. 41
30. D. Tichit, A. Rolland, F. Prinetto, G. Fetter, M.J. Martínez-Ortíz, M.A. Valenzuela et al., J. Mater. Chem. **12**, 3832 (2002). doi:10.1039/b203376n